Supporting Information

AFM nanomanipulation of shape persistent, spherical, self-assembled gold nanoparticles

Jeroen van Herrikhuyzen, [†] Ron Willems, [†] Subi J. George, [†] Cees Flipse, [†] Jeroen C. Gielen,[‡] Peter C.M. Christianen, [‡] Albertus P. H. J. Schenning,[†,*] Stefan C. J. Meskers [†,*]

[†] Laboratory for Macromolecular and Organic Chemistry, Eindhoven University of Technology, PO Box 513, 5600MB Eindhoven, The Netherlands,

[‡] High Field Magnet Laboratory, Institute for Molecules and Materials, Radboud University Nijmegen, Toernooiveld 7, 6525 ED Nijmegen, The Netherlands,

Address correspondence to s.c.j.meskers@tue.nl, a.p.h.j.schenning@tue.nl

General methods

Nuclear magnetic resonance spectroscopy (NMR). ^{1}H NMR and ^{13}C NMR spectra were recorded in $CDCl_3$ at 25.0 °C on a Varian Mercury Vx (400 MHz). Additionally ^{1}H-^{1}H COSY and HETCOR experiments were carried out to assign all peaks. Chemical shifts (δ) are given in ppm relative to tetramethylsilane, which was used as internal standard. Abbreviations used are s = singlet, d = doublet, t = triplet, m = multiplet and br = broad.

Infrared spectroscopy (IR). Infrared spectra were run on a Perkin Elmer Spectrum One UATR FT-IR spectrophotometer.

Mass spectroscopy (MS). MALDI-TOF MS spectra were measured on a Perspective DE Voyager spectrometer utilising an α-cyano-4-hydroxycinnamic acid matrix; mode of operation: reflector; polarity: positive.

Elemental analysis. Elemental analysis was carried out on a Perkin Elmer 2400 series II CHNS/O analyzer.

Optical spectroscopy. UV/Vis measurements were performed on a Perkin Elmer Lambda 40 UV/Vis Spectrometer or a Perkin Elmer Lambda 900 UV/Vis/NIR Spectrometer. Fluorescence measurements were performed on a Edinburgh Instruments FS920 double-monochromator luminescence spectrometer using a Peltier-cooled red-sensitive photomultiplier.

Transmission electron microscopy (TEM). TEM grids, both 200 mesh carbon-coated copper grids and R2/2 Quantifoil Jena grids were purchased from Aurion. Samples were prepared by applying a droplet of sample solution onto the grid, and then blotting away the excess solution using a filter paper. The samples were analysed at room temperature on a FEI Tecnai 20, type Sphera TEM operating with a 200 kV LaB6 filament, equipped with a bottom mounted 1k × 1k Gatan CCD camera.

Atomic force microscopy (AFM). Atomic force microscopy (AFM) measurements were carried out at room temperature with an AFM (Digital Instruments) equipped with a Nanoscope IIIa controller (Digital Instruments) in the Tapping Mode. Substrates were cleaned intensively by rinsing with acetone and ethanol followed by drying under nitrogen flow.

Dynamic light scattering (DLS). DLS measurements were carried out using an intensity-stabilized helium-neon laser (Spectra Physics, λ=632.8 nm, 4.5 mW). The incident beam of the laser was focused in the center of a cylindrical glass cell (Helma). The light, scattered at 90° with respect to the incident beam, was transferred to a single photon detector (ALV/SO-SIPD) through a single mode fiber to meet the spatial coherence conditions. The signal was processed with a 320-channel Multiple Tau Digital Correlator (ALV-5000/E). The measurements were carried out in a

temperature range of 23-90 °C (± 0.05 °C) using a laboratory-made heating stage driven by an active feedback temperature controller (LakeShore 340).

Intensity fluctuations in the scattered light detected in a small volume and on a microsecond timescale are related to the Brownian motion of the particles due to density fluctuations. The normalized autocorrelation function of the intensity of the scattered light is given by:

$$g^{(2)}(\tau) = \frac{\langle I(t)I(t+\tau)\rangle}{\langle I(t)I(t)\rangle} = \frac{\langle n(t)n(t+\tau)\rangle}{\langle n(t)n(t)\rangle} \quad (1)$$

where $I(t)$ is the intensity of the scattered light at time t and $n(t)$ is the photon count number detected at time t. This function can be expressed as:

$$g^{(2)}(\tau) = 1 + \beta\left|g^{(1)}(\tau)\right|^2 \quad (2)$$

where

$$g^{(1)}(\tau) = \frac{\langle E(t)E^*(t+\tau)\rangle}{\langle E(t)E^*(t)\rangle} \quad (3)$$

is the time autocorrelation function of the electric field of the scattered light, β is a factor that depends on the experimental set-up and $\langle\ \rangle$ indicates averaging over t.

For an ensemble of monodisperse spherical particles under translational Brownian motion, the autocorrelation function $g^{(1)}(\tau)$ decays exponentially on time.

$$g^{(1)}(\tau) = \exp(-Dq^2\tau) \quad (4)$$

where q is the scattering vector

$$q = \frac{4\pi n}{\lambda}\sin\left(\frac{\theta}{2}\right) \quad (5)$$

with n is the refractive index of the solvent, λ the wavelength of the incident light, θ the scattering angle and D the translational diffusion coefficient. By fitting the experimental correlation function by equation 4, D was determined, from which the hydrodynamic radius R_H of the diffusing particles was calculated from the Stokes-Einstein relationship

$$R_H = \frac{k_B T}{6\pi\eta D} \quad (6)$$

where k_BT is the thermal energy and η the, temperature dependent, viscosity of the suspending medium.

Synthesis.

The synthesis of the **OPV1-Au** particles having an average diameter of 2.4 nm has been reported previously.[S1]

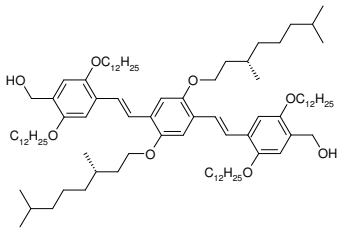

OPV3

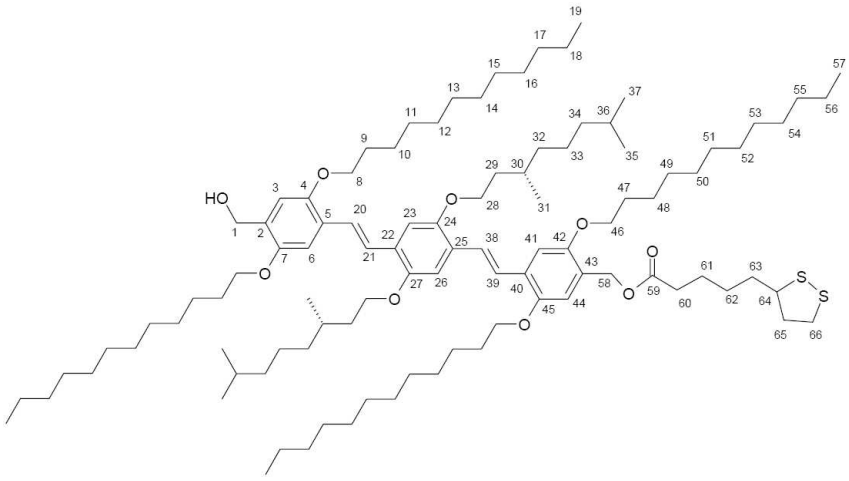

OPV2

5-[1,2]Dithiolan-3-ylpentanoic Acid (E,E)-4-{4-(2,5-bisdodecyloxy-4-hydroxymethyl-styryl)-2,5-bis[(S)-3,7-dimethyloctoxy-styryl}-2,5-bisdodecyloxybenzyl Ester (OPV2).

200 mg (0.14 mmol) Bisalcohol **OPV3**[S2] and 40 mg (0.20 mmol) thioctic acid were dissolved in 50 mL chloroform. The mixture was stirred for 15 minutes at 0 °C under an argon atmosphere. Then a solution of 42 (0.22 mmol) mg 1-ethyl-3-(3-dimethylaminopropyl) carbodiimide hydrochloride (EDC) and 16 mg (0.12 mmol) 4-(dimethylamino)-pyridine (DMAP) in 5 mL dichloromethane was added and stirring was continued at 0 °C for another 15 minutes. Stirring for an additional 24 hours at

room temperature gave a mixture of **OPV3**, **OPV2** and the bis-functionalised product. Then the reaction mixture was washed three times with water, dried over anhydrous MgSO4 and evaporated *in vacuo*. Purification by column chromatography on silica gel (methanol/chloroform (0.5-1.5):(99.5-98.5)) and precipitation from methanol yielded pure **OPV2** (90 mg, 40 %).

^{1}H-NMR (400 MHz, CDCl3, 25 °C, TMS): δ 0.88 (m, 24 H, *19*, *35*, *37* and *57*), 0.97 (d, 6 H, *31*), 1.12 - 1.91 (m, 109 H, *9* - *18*, *29*, *30*, *32* - *34*, *36*, *47* - *56* and *65*), 2.38 (t, *J* = 7.6 Hz, 2 H, *60*), 2.45 (m, 1 H, *65*), 3.15 (m, 2 H, *66*), 3.55 (m, 1 H, *64*), 3.96 - 4.10 (m, 12 H, *8*, *28* and *46*), 4.68 (d, 2 H, *1*), 5.16 (s, 2 H, *58*), 6.87 (s, 1 H, *3*), 6.89 (s, 1 H, *44*), 7.12 (s, 2 H, *6* and *41*), 7.14 (s, 2 H, *23* and *26*), 7.46 (s, 4 H, *20*, *21*, *38* and *39*).

^{13}C-NMR (100 MHz, CDCl3, 25 °C, TMS): δ {14.46, 20.20, 22.93, 23.03, 25.10, 26.52, 26.57, 26.60, 28.31, 29.12, 29.71, 29.80, 29.84, 29.98, 30.02, 30.56, 32.27, 34.52, 44.97, 35.78, 36.89, 37.76, 38.83, 39.65, 40.54} (68 C, *9* - *19*, *29* - *37*, *47* - *57*, *60* - *63*, *65* and *66*), 56.67 (1 C, *64*), 62.08 (1 C, *58*), 62.68 (1 C, *1*), {68.15, 68.91, 69.26, 70.04} (6 C, *8*, *28* and *46*), {109.31, 109.86, 110.72, 110.79, 114.35, 115.45} (6 C, *3*, *6*, *23*, *26*, *41* and *44*), {123.48, 123.62, 123.73, 124.17, 124.77, 127.54, 127.75, 128.53, 129.69} (10 C, *2*, *5*, *20*, *21*, *22*, *25*, *38, 39, 40* and *43*), {150.81, 150.98, 151.34, 151.40, 151.44, 151.73} (6 C, *4*, *7*, *24*, *27*, *42* and *45*), 173.75 (1 C, *59*).

IR (UATR): *v* (cm-1): 2921, 2852 (C-H stretch); 1730 (C=O stretch); 1509, 1467, 1421, 1390, 1343, 1253, 1205, 1050, 1001, 965, 855, 720.

MALDI-TOF-MS (FW = 1580.59): m/z: 1580.18 [M]+.

Synthesis and Characterization of OPV-Gold particles

For the decoration of gold nanoparticles with OPVs two routes have been used, giving average diameters for the gold core of 2.4 and 4.1 nm respectively.[S3]

In the first, direct method (method a in Figure S1), the gold nanoparticle precursor $HAuCl_4 \cdot 3H_2O$ was dissolved in water and subsequently phase-transferred to toluene by means of tetra-*n*-octylammonium bromide (**TOAB**). This resulted in a colour change from yellow to red, as droplets of water containing Au^{3+} were dispersed in toluene by the amphiphilic molecules. Next, a thiol (*e.g.* **OPV1** or **OPV2**) was added, followed by a freshly prepared aqueous solution of $NaBH_4$ while stirring vigorously. Immediately the solution darkened and started to bubble, indicating the reduction of Au^{3+} ions to Au^0 and the formation of **OPV-Au** nanoparticles. When the reaction was completed, the nanoparticles were washed extensively with ethanol and then acetone, in order to remove the excess of unbound **OPV** ligands and **TOAB** surfactants. The nanoparticles are stable enough for preparative size-exclusion chromatography (Biobeads) and this was used to remove unbound ligands. After purification, the OPV-gold nanoparticles were characterised by a variety of techniques (see main text).[S4]

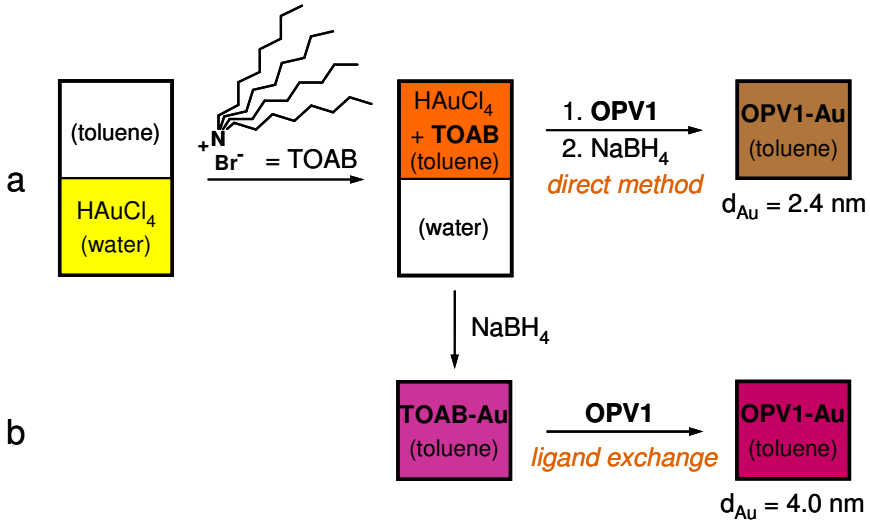

Figure S1. Two synthetic routes to **OPV1-Au** nanoparticles with different d_{Au}.

In the second method $HAuCl_4 \cdot 3H_2O$ is reduced in the absence of thiol molecules, yielding gold nanoparticles stabilised by **TOAB** surfactants (**TOAB-Au**, method b in Figure S1). The diameters of such particles are larger than the ones prepared by method a. By subsequently adding thiol derivatives (*e.g.* **OPV1** or **OPV2**), the **TOAB** ligands could be exchanged, resulting in thiol-functionalised **OPV-Au** nanoparticles, which were purified in the same fashion as for method a. For the characterization of these particles see main text.

AFM nanomanipulation.

For imaging, a Dimension 3100, Veeco Instruments Inc., U.S.A., Scanning ProbeMicroscope, with a NanoScope IIIa controller, is used together with NSC35 AFM cantilevers (with resonance frequencies between 240 and 405 kHz and force constants between 6.5 and 27.5 N/m) from MikroMasch, Estonia. Moving the aggregates across the substrate was done with the abovementioned AFM, NSC35 cantilevers and a home-build script for the Nanoscope control software.

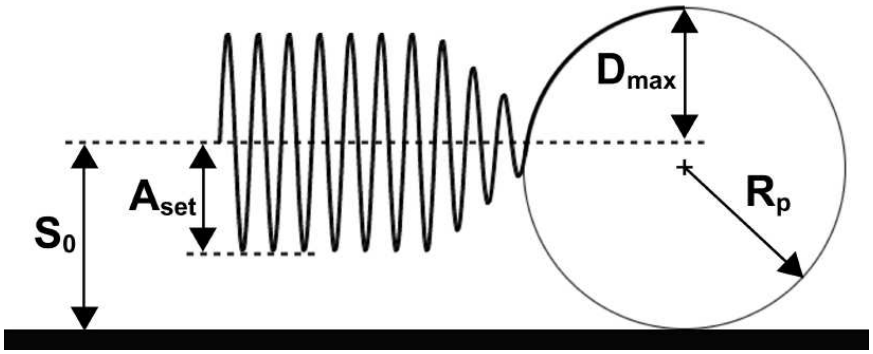

Figure S2. Moving a particle with tapping-mode AFM. As the tip approaches the particle the oscillation amplitude decreases and eventually the cantilever starts to deflect. The deflection indicates that force is being applied to the particle. If the deflection is large enough, the applied forces will be greater than the forces with which the particle clings the surface and the particle will be displaced. In this image A_{set} is the amplitude-setpoint, S_0 the (zero-amplitude) tip-substrate separation, R_p the radius of the particle and D_{max} the maximum reflection the cantilever can experience in this situation.

Besides imaging of the substrate, AFM has been used to manipulate aggregates on the substrate. Figure S2 gives a qualitative picture of what happens during an attempt to move an aggregate. The free oscillation amplitude A_{free} of the tip is set to a specific (but for this discussion arbitrary) value. If the feed-back loop is on, then by setting the (oscillation) amplitude-setpoint A_{set} to a value lower than A_{free}, the tip will move closer to the surface, causing the surface forces acting on the tip to decrease the oscillation amplitude until A_{set} is reached. The (zero-amplitude) tip-sample separation

at which this happens is called S_0. The exact value of S_0 is not known, but is dependent on A_{free} and A_{set}. By turning the feed-back loop off, S_0 becomes a fixed distance. If the tip is now scanned over the surface, then as long as the (zero-amplitude) tip sample separation remains constant (and equal to S_0), the oscillation amplitude will remain the same as well. However, as the tip approaches a particle, the tip-sample separation becomes smaller, causing the oscillation amplitude to decrease. When this oscillation dies out (the tip hits the particle), the cantilever starts to deflect. Deflection of the cantilever indicates that the tip applies a force to the particle, and the bigger the deflection, the larger the applied force will be. If this force becomes big enough, i.e bigger than the forces holding the particle to the surface, then the particle will be moved.[S5,S6,S7]

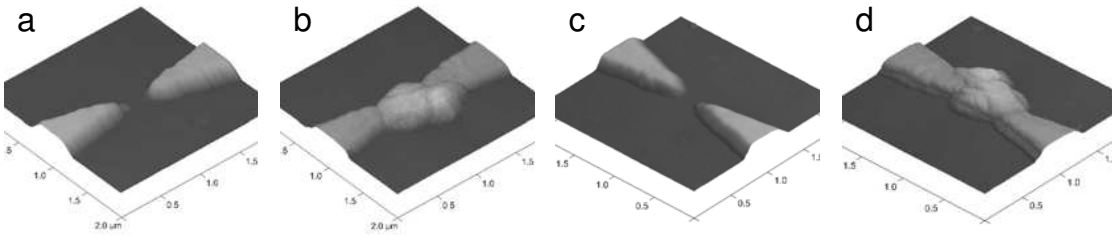

Figure S3. 3-D AFM images projected from two different angles (a-b and c-d, respectively) of the aggregate of 2.4 nm **OPV1-Au** particles pushed in between electrodes (see also Figure 5) after deposition from *n*-heptane (2×10^{-5} M) on a octadecyltrichlorosilane-coated SiO_2 surface.

Self-assembly of OPV-Au aggregates without a hydroxy functionality.

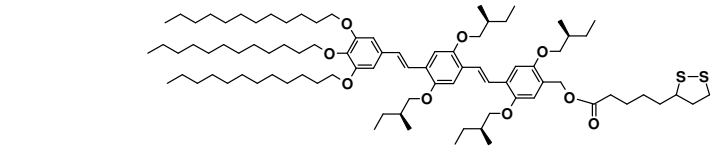

OPV 4

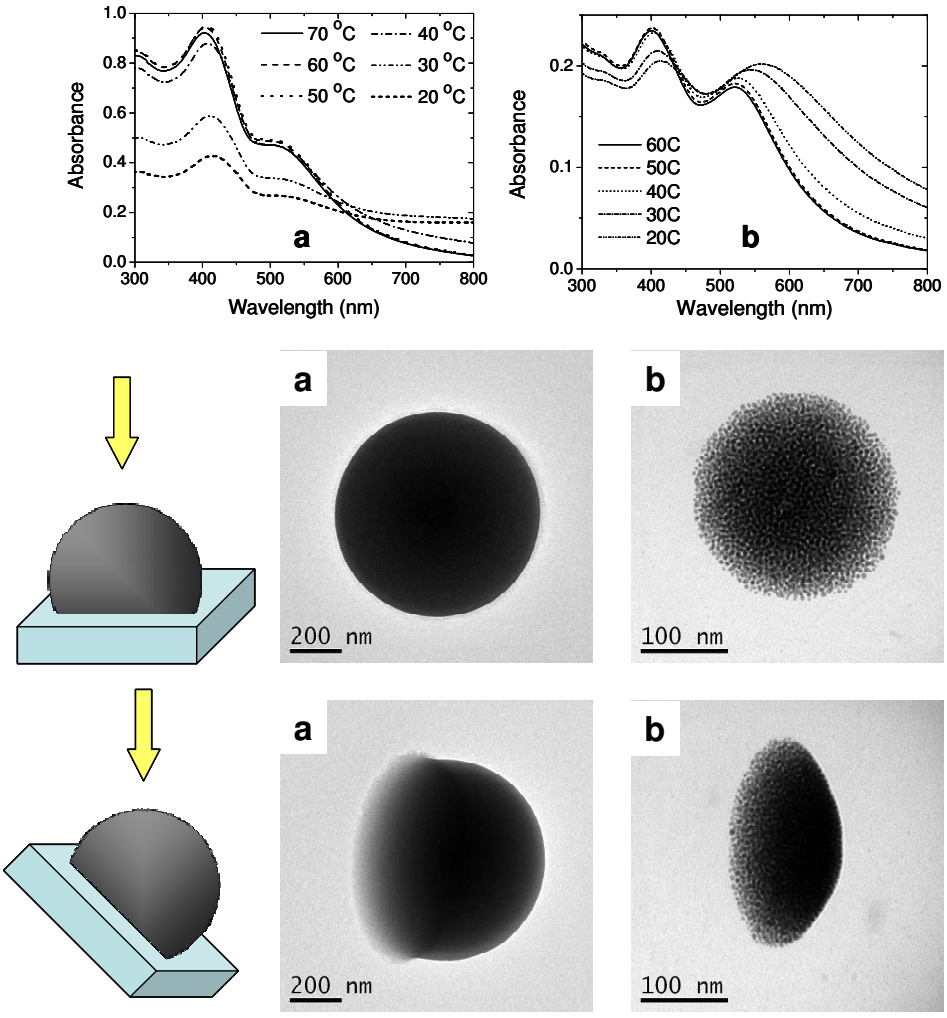

Figure S4. Self-assembly behavior of **OPV2-Au** nanoparticles, d_{Au}= 2.4 nm at concentrations of 2 × 10^{-5} M in *n*-heptane (a), Self-assembly of **OPV4-Au** nanoparticles,[S3] with d_{Au}= 4.1 nm, cast from 0.1 μM solution in *n*-butanol. Upper row: optical characterization. Lower rows: TEM images at different tilt angle (0 and 60°).

References

S1 van Herrikhuyzen, J.; George, S.J.; Vos, M.R.J.; Sommerdijk, N.A.J.M.; Ajayaghosh, A.; Meskers, S.C.J.;. Schenning, A.P.H.J. *Angew. Chem. Int. Ed.* **2007**, 46, 1825 –1828.

S2 George, S. J.; Ajayaghosh, A.; Jonkheijm, P.; Schenning, A. P. H. J.; Meijer, E. W.. *Angew. Chem. Int. Ed.* **2004**, *43*, 3422 –3425.

S3 van Herrikhuyzen, J.; Janssen, R.A.J.; Meijer, E.W.; Meskers, S.C.J.; Schenning, A.P.H.J. *J. Am. Chem. Soc.*, **2006**, *128*, 686-687.

S4. Jonkheijm, P. ; Hoeben, F. J. M.; Kleppinger, R.; van Herrikhuyzen, J.; Schenning, A. P. H. J.; Meijer, E. W. *J. Am. Chem. Soc.* **2003**, *125*, 15941 – 15949.

S5. Resch, R. ; Bugacov, A.; Baur, C.; Koel, B. E.; Madhukar, A.; Requicha, A. A. G.;Will, P. 'Manipulation of nanoparticles using dynamic force microscopy: simulation and experiments', Applied Physics A, **1998,** *67*, 265–271.

S6. Requicha, A. A. G.; Meltzer, S.; Teran Arce, F. P.; Makaliwe, J. H.; Siken, H. ; Hsieh, S.; Lewis, D.; Koel, B. E.; Thompson, M. 'Manipulation of nanoscale components with the AFM: principles and applications', in 'EEE Int'l Conf. on Nanotechnology', **2001**, 28–30.

S7. (a) Bugacov, A.; Resch, R.; Baur, C.; Montoya, N.; Woronowicz, K.; Papson, A.; Koel, B.E.; Requicha A.; Will, P. 'Measuring the tip-sample separation in dynamic force microscopy', *Probe Microscopy*, **1999**, 1; (b) Mazer, N. A.; Benedek, G. B.; Carey, M. C. *Biochemistry* **1980**, *19*, 601 – 615.